Clim. Past Discuss., 11, 2077–2119, 2015
www.clim-past-discuss.net/11/2077/2015/
doi:10.5194/cpd-11-2077-2015
© Author(s) 2015. CC Attribution 3.0 License.

Climate of the Past Discussions
Open Access

This discussion paper is/has been under review for the journal Climate of the Past (CP).
Please refer to the corresponding final paper in CP if available.

Stratification of surface waters during the last glacial millennial climatic events: a key factor in subsurface and deep water mass dynamics

M. Wary[1], F. Eynaud[1], S. Marjolaine[1], S. Zaragosi[1], L. Rossignol[1], B. Malaizé[1], E. Palis[1,*], J. Zumaque[1,], C. Caulle[1,***], A. Penaud[2], E. Michel[3], and K. Charlier[1]**

[1]UMR5805, EPOC (Environnements et Paléoenvironnements Océaniques), Université de Bordeaux, 33615 Pessac, France
[2]UMR6538, Domaines Océaniques, IUEM-UBO, 29280 Plouzané France
[3]UMR8212, LSCE (Laboratoire des Sciences du Climat et de l'Environnement), CEA/CNRS-INSU/UVSQ, 91198 Gif-sur-Yvette CEDEX, France
[*]now at: UMR7329, Géoazur, Université de Sophia Antipolis, 06560 Valbonne, France
[**]now at: UQAM, Université du Québec à Montreal, Montréal, Québec H3C 3P8, Canada
[***]now at: Laboratory of Recent and Fossil Bio-Indicators, CNRS UMR6112 LPG-BIAF, Angers, France

Received: 25 April 2015 – Accepted: 8 May 2015 – Published: 29 May 2015

Correspondence to: M. Wary (melanie.wary@u-bordeaux.fr)

Published by Copernicus Publications on behalf of the European Geosciences Union.

CPD
11, 2077–2119, 2015

Abstract

The last glacial period was punctuated by abrupt climatic events with extrema known as Heinrich Events and Dansgaard–Oeschger cycles. These millennial events have been the subject of many paleoreconstructions and model experiments in the past decades, but yet the hydrological processes involved remain elusive. In the present work, high resolution analyses were conducted on the 12–42 ka BP section of core MD99-2281 retrieved Southwest off Faeroes. Our multiproxy approach, coupling micropaleontological, geochemical and sedimentological analyses, allows us to track surface, subsurface, and deep hydrological processes occurring during these rapid climatic changes. Records indicate that the coldest episodes of the studied period (Greenland stadials and Heinrich stadials) were characterized by a strong stratification of surface waters. This surface stratification seems to have played a key role in the dynamics of subsurface and deep water masses. Indeed, periods of high surface stratification are marked by a coupling of subsurface and deep circulations which sharply weaken at the beginning of stadials while surface conditions progressively deteriorate throughout these cold episodes; at the opposite, periods of decreasing surface stratification (Greenland interstadials) are characterized by a coupling of surface and deep hydrological processes with progressively milder surface conditions and gradual intensification of the deep circulation while the vigor of the subsurface Atlantic inflow remains constantly high. Our results also reveal different and atypical hydrological signatures during Heinrich stadials (HS): while HS1 and HS4 exhibit a "usual" scheme with reduced overturning circulation, a relatively active North Atlantic circulation seems to have prevailed during HS2, and HS3 seems to have experienced a re-intensification of this circulation at mid-event. Our findings thus bring valuable information to better understand hydrological processes occurring in a key area during the abrupt climatic shifts of the last glacial period.

CPD
11, 2077–2119, 2015

1 Introduction

The last glacial period (~ 60–10 ka BP) is characterized by abrupt climate oscillations. This millennial to sub-millennial climatic variability was first evidenced in Greenland atmospheric temperature records as oscillations occurring every 1–4 ka and known as Dansgaard–Oeschger events (DO) (Dansgaard et al., 1993; Bond et al., 1993). DO events are characterized by a rapid transition occurring in a few decades from cold (Greenland stadial – GS) to warm (Greenland interstadial – GIS) conditions. These events have been widely identified in marine archives from the subpolar North Atlantic Ocean and adjacent seas as coeval changes in surface and deep hydrology (e.g. Rasmussen et al., 1996a, b; Kissel et al., 1999; Van Kreveld et al., 2000; Rahmstorf, 2002). Moreover, during GS (including the most massive, i.e. Heinrich stadials – HS), increases of iceberg and ice-rafted debris (IRD) delivery from the boreal ice-sheets are recorded (e.g. Heinrich, 1988; Bond et al., 1992; Bond and Lotti, 1995; Elliot et al., 2001). Despite a large number of paleoreconstructions and model experiments focusing on this millennial climatic variability, processes involved still remain elusive and different mechanisms are invoked. Most of the preconized theories involve changes in the meridional overturning circulation, either as the cause (e.g. Alvarez-Solas et al., 2010) or the consequence (e.g. Manabe and Stouffer, 1995; Ganopolski and Rahmstorf, 2001; Levine and Bigg, 2008) of these periodic ice-sheet instabilities.

In order to better understand these phenomena, the importance of working on high resolution records coming from key locations has been highlighted. Previous studies of marine cores located around major sills in between the North Atlantic Ocean and the Nordic Seas have shown the strong potential of this buffer area to track this variability (see references herein). Most of these studies agree with coeval oscillations of the meridional overturning circulation, depicted as weaker loop of Atlantic inflow and deep overflow from the Nordic Seas during GS and HS and inversely during GIS (e.g. Rasmussen et al., 1996a, b, 2002a; Moros et al., 1997, 2002; Kissel et al., 1999, 2008; Van Kreveld et al., 2000; Elliot et al., 2002; Rasmussen and Thomsen, 2004; Ballini

CPD
11, 2077–2119, 2015

et al., 2006; Dickson et al., 2008). Some of them (Rasmussen et al., 1996a, b; Rasmussen and Thomsen, 2004; Van Kreveld et al., 2000; Dokken et al., 2013), on the basis of indirect proxies of sea surface conditions, suggest a strong stratification of the water column and the presence of a halocline during GS, which might have affected the oceanic circulation at greater depths.

Our study uses a direct proxy of surface sensu stricto conditions, i.e. dinoflagellate cyst (dinocyst) assemblages, coupled to other proxies that give access to subsurface (foraminifera assemblages and geochemical analyses on their shells) and deep water mass dynamics (sediment grain-size measurements and magnetic susceptibility). Analyses were conducted at a high temporal resolution (i.e. centennial to millennial) on core MD99-2281 located southwest off Faeroes Islands. This multiproxy approach allows us (i) to directly evidence the past water-mass structure and especially if stratification did occur, (ii) to track this stratification evolution during the millennial abrupt events, and (iii) to evaluate its influence on subsurface and bottom circulations.

2 Environmental setting and paleoceanographic interests

Core MD99-2281 (60.3418° N, −9.4557° E, 1197 m water depth) was retrieved during the IMAGES V – GINNA cruise on the RV *Marion Dufresne* (Labeyrie et al., 1999). The coring site is located southwest off Faeroes, at the southern foot of the Faeroe Bank and north of the Rockall Trough (Fig. 1).

This area constitutes a nodal point regarding modern oceanic circulation, as it is influenced by (i) the warm and salty Atlantic surface waters ($T > 5\,^{\circ}C$, $S > 35.0$; Hansen and Osterhus, 2000) conveyed by the poleward current of the North Atlantic Drift (NAD), and (ii) the deep, cold and less saline waters ($T < 3\,^{\circ}C$, $S < 35.0$; Hansen and Osterhus, 2000) overflowing from the Nordic Seas (e.g. Kuijpers et al., 1998a, b, 2002; Rasmussen et al., 2002b; Zumaque et al., 2012; Caulle et al., 2013) (Fig. 1). At present, the Norwegian Sea Overflow Water (NSOW), one component of these deep water-masses, flows southward from its formation area (i.e. the Norwegian sea) through the Faeroe–

CPD
11, 2077–2119, 2015

Shetland Channel and then is divided into two branches: a northern and permanent branch, and a southern and non-permanent one (Fig. 1b). Our site is located beneath the southern branch, which intermittently crosses the Wyville–Thompson Ridge (a topographic barrier culminating at around 600 m water-depth) and flows southward (e.g. Boldreel et al., 1998; Kuijpers et al., 1998a, b, 2002; Zumaque et al., 2012; Caulle et al., 2013). Nevertheless, according to Boldreel et al. (1998), the coring site is located within the area unaffected by strong current activities, with sedimentation resulting from pelagic sediments deposited in a low-energy, deep-water environment.

This system of water-mass exchange is known to have been very sensitive to the millennial-scale climatic variability of the last glacial period (e.g. Rasmussen et al., 1996a, b, 2002a; Moros et al., 1997, 2002; Kissel et al., 1999, 2008; Van Kreveld et al., 2000; Elliot et al., 2002; Eynaud et al., 2002; Rasmussen and Thomsen, 2004, 2008; Ballini et al., 2006; Dickson et al., 2008; Zumaque et al., 2012; Caulle et al., 2013). This is particularly true for the Faeroe region which was then under the direct influence of the proximal European ice-sheets (i.e. the Fennoscandian and the British–Irish ice-sheets; Fig. 1a) whose decays/built-up have modulated the oceanic and climatic dynamics. Therefore, core MD99-2281 is expected to have recorded changes in the vigor of the NAD penetration and NSOW overflow in relation to European ice-sheets history.

3 Material and methods

3.1 Stratigraphy of the core

The age model of core MD99-2281 conforms to the previous published one from Zumaque et al. (2012) and Caulle et al. (2013). As preconized by several paleoceanographic studies in this area (e.g. Kissel et al., 1999, 2008; Laj et al., 2000; Elliot et al., 2002; Eynaud et al., 2002; Ballini et al., 2006; Rasmussen and Thomsen, 2009; Dokken et al., 2013), the age model is constrained by 10 AMS ^{14}C dates measured on planktonic foraminifera monospecific samples, combined to 18 additional tie-points obtained

CPD
11, 2077–2119, 2015

by comparing the magnetic susceptibility record of core MD99-2281 to the $\delta^{18}O$ signal of NGRIP ice-core (GICC05 time scale; Andersen et al., 2006; Svensson et al., 2008; Wolff et al., 2010; see Figs. 2–5 where dates are illustrated by red stars and tie-points by blue stars along the age axis). The age model was finally established on the basis of a linear interpolation between ages and tie-points (see Zumaque et al., 2012 for further explanations). It is important to note that supplementary stratigraphic control points, independent from climate, were retrieved from the record of the changes in the Earth's magnetic field (analysis performed at the LSCE), namely the Mono Lake and the Laschamps events. Those additional tie points give confidence in the established age model (see Fig. 4 in Zumaque et al., 2012).

The coring site experienced relatively high sedimentation rates during the last glacial period (between 23 and 408 cm ka^{-1}, with a mean around 61 cm ka^{-1} for the studied section, i.e. 300–2090 cm or ~ 12–42 ka cal BP, cf. Fig. 4). These rates, combined to our sampling frequency (every ~ 10 cm on the studied section for all analyses except for grain size analyses on a short portion of the core and for magnetic susceptibility measurements, cf. Sect. 3.5.), lead to appropriate degrees of temporal resolution (between ~ 25 and ~ 525 years, with a mean of ~ 165 years) to study the last glacial rapid climatic variability at an infra-millennial scale.

3.2 Organic-walled dinoflagellate cysts (dinocysts)

Dinocyst specific determination and counting were performed within the framework of two previous studies: Caulle et al. (2013) for the 12–27 ka BP section of the studied core, and Zumaque et al. (2012) for the 27–42 ka BP section. Methods for palynological preparation, identification, counts and calculations of abundances are described in these two studies. Data stemming from those analyses are the concentration of modern (i.e. Quaternary) dinocysts (number of cysts cm^{-3} of dried sediment), dinocyst assemblages described with the relative abundances of each species (relative to the total number of specimens including unidentified taxa and excluding reworked, i.e. pre-

CPD
11, 2077–2119, 2015

Quaternary, dinocysts), and the concentration of coenobia of freshwater micro-algae *Pediastrum* spp.

Past sea-surface conditions were estimated using a transfer function applied to dinocyst assemblages. The modern analogue technique (MAT, see Guiot and de Vernal, 2007, 2011a, b for a review of this technique) was applied and performed with the R software (R version 2.7.0; http://www.r-project.org/), using the ReconstMAT script developed by J. Guiot (BIOINDIC package, https://www.eccorev.fr/spip.php?article389). The modern dinocyst database used here includes 1189 sites from North Atlantic Ocean, Arctic and sub-Arctic basins, Mediterranean Sea and North Pacific Ocean (DINO9 meeting, 2011; see the following website www.geotop.ca/ for the successive implementation of the database). These statistical treatments provide quantitative reconstructions for various hydrological parameters, among which are mean summer (July–August–September) and mean winter (January–February–March) sea-surface temperatures (SST) (with root mean square errors of prediction – RMSEP – of 1.5 and 1.05 °C respectively), mean summer and mean winter sea-surface salinities (SSS; respective RMSEP of 2.4 and 2.3 psu; see Caulle et al., 2013 and Zumaque et al., 2012 for further details).

3.3 Planktonic foraminifera

Planktonic foraminifera analyses were performed on the > 150 µm fraction, on the same samples as those used for dinocyst analyses. A minimum of 350 specimens sample^{-1} were identified and counted. Abundances of each species were calculated relative to the total sum of planktonic foraminifera. Counts of total benthic foraminifera were also performed, and planktonic and benthic foraminifera total concentrations (number of specimen g^{-1} of dried sediment) were calculated.

In order to obtain quantitative temperature reconstructions for the layer of the water column inhabited by planktonic foraminifera (hereafter "F-Temp" for "foraminifera-derived temperatures"), the MAT was applied to the relative abundances using, as for dinocysts, the R software and the ReconstMAT script. In this case, quantifications rely

CPD
11, 2077–2119, 2015

on a weighted average of SST values associated with the five best modern analogues selected in a database including modern assemblages from 1007 sites distributed over the North Atlantic Ocean and Mediterranean Sea (see Eynaud et al., 2013 for details regarding this database and the associated MAT). This method allows us to reconstruct mean summer (July–August–September) and mean winter (January–February–March) F-Temp with RMSEP of 1.3 and 1.2 °C respectively.

Stable isotope measurements ($\delta^{18}O$) were also performed on monospecific samples of *Neogloboquadrina pachyderma* sinistral coiling. For each sample (the same as those used for F-Temp reconstructions), 5 to 6 specimens (i.e. ~ 65 µg mean weight aliquots) were hand-picked from the 200–250 µm size fraction. From 300 to 1190 cm (~ 12–27 ka BP, 90 samples) measurements were done at LSCE laboratory using a Finnigan MAT 251 mass spectrometer. The mean external reproducibility of carbonate standard NBS19 was ±0.05 ‰. From 1200 to 2090 cm (~ 27–42 ka BP, 90 samples), measurements were performed at EPOC laboratory with an Optima Micromass mass spectrometer. Reproducibility of NBS19 was ±0.03 ‰. Those two spectrometers are intercalibrated thus allowing us to directly compare both records. In both cases, values are given vs. Vienna Pee Dee Belemnite (VPDB) standard.

To estimate past changes in seawater isotopic composition ($\delta^{18}O_{SW}$), we used the paleotemperature equation developed by Epstein and Mayeda (1953) and Shackleton (1974) which links the $\delta^{18}O_{SW}$, the isotopic composition of calcareous shells ($\delta^{18}O_C$) and the calcification temperature (T) as follows: $T = 16.9–4.38\ (\delta^{18}O_C - \delta^{18}O_{SW}) + 0.13\ (\delta^{18}O_C - \delta^{18}O_{SW})^2$. Following Duplessy et al. (1991), we used $\delta^{18}O$ measurements on *N. pachyderma* s. as $\delta^{18}O_C$, and mean summer F-Temp corrected by 2.5 °C as T. We then followed the method recently described in Malaizé and Caley (2009) to extract the $\delta^{18}O_{SW}$ signal. Variations of this signal depend on past fluctuations of local salinities as well as on the global isotopic signal related to changes in continental ice-sheet volume. We used the global $\delta^{18}O$ signal of Waelbroeck et al. (2002) to remove $\delta^{18}O$ variations due to glacial–interglacial ice volume changes. We thus obtained a local $\delta^{18}O_{SW}$ signal that can be used as an indicator of local salinities changes.

CPD
11, 2077–2119, 2015

Nevertheless, it should be kept in mind that this signal is not corrected from the rapid ice volume fluctuations associated with Marine Isotopic Stage 3 (MIS3) collapse events, those fluctuations still remaining not fully understood and discrepancies still existing between the various sea-level reconstructions (Siddall et al., 2008). Quantitative estimations of salinities were not carried out as large uncertainties remain concerning the temporal stability of the relation linking local $\delta^{18}O_{SW}$ to salinity, even if a recent study, using atmospheric isotopic model, tends to minimize these uncertainties within our study area (Caley and Roche, 2013).

3.4 Ecological indices

Some ecological indices were calculated both on dinocyst and planktonic foraminifera assemblages. Diversity is represented by the H index: $-\sum_{i=1}^{s}[(n_i/N)\cdot\ln(ni/N)]$, where n_i is the number of specimens recorded for taxa i, s the total number of taxa and N the total number of individuals counted for each sample (Shannon and Weaver, 1949). Dominance corresponds to $(n' + n'')/N$ where n' is the number of individuals of the more abundant species, n'' the number of individuals of the second more abundant species, and N the total number of specimens counted for each sample (cf. Goodman, 1979).

3.5 Sedimentological proxies

Magnetic Susceptibility was measured onboard every 2 cm with a GEOTEK Multi-Sensor Core Logger (Labeyrie and Cortijo, 2005). More detailed magnetic analyses were performed at the LSCE with a 45 mm diameter MS2-C Bartington coil on the MIS 3 section (see Zumaque et al., 2012). However, as the present study also focuses on MIS 2, we chose to present the continuous onboard signal which is furthermore very similar to the low field magnetic susceptibility record obtained at the LSCE (see Fig. 3 in Zumaque et al., 2012).

CPD
11, 2077–2119, 2015

Grain-size measurements were performed on a Malvern MASTER SIZER S at EPOC laboratory (University of Bordeaux). Subsamples of bulk sediment were taken every ~ 10 cm between 40 and 2170 cm (~ 11–43 ka BP), except between 1791.5 and 1940.5 cm (~ 37–40 ka BP) where sampling was done every centimeter (371 samples in total); those subsamples did not receive any chemical pretreatment before being analyzed. But to ensure that results obtained from non-pretreated sediment mainly reflect grain-size variations of the terrigenous fraction in our study area, a second set of analyses was conducted on carbonate-free and organic-free subsamples (pretreatment with HCl 10 % and H_2O_2 35 %) taken every ~ 10 cm from 1593 to 1791 cm (~ 33.6–37 ka BP, same depth as the non-pretreated subsamples). Results derived from the bulk subsamples will be further represented as a mapping of the relative percentages of the different grain-size fractions along core. Some grain-size parameters were additionally calculated: median (D50), percentiles 10 and 90 (D10 and D90), mean grain size of the 10–63 µm fraction, mode, and silt ratio. The mode corresponds to the mean diameter of the most abundant size fraction. The silt ratio, reflecting size variations in the silt fraction, corresponds to the ratio of the percentage of the coarse silt fraction (26–63 µm) over the percentage of the fine silt fraction (10–26 µm).

Large Lithic Grains (LLG) concentrations (nb. of grains g^{-1} of dry sediment) were determined in the > 150 µm sediment fraction of the studied core, in the same samples as those used for foraminifera and dinocyst analyses. As in many works conducted in the study area (e.g. Elliot et al., 1998, 2001; Rasmussen et al., 2002a; Scourse et al., 2009), we assume that LLG contain a large proportion of ice-rafted debris, and thus consider this proxy as an indicator of floating ice (i.e. icebergs or coastal sea-ice) delivery to the site.

CPD
11, 2077–2119, 2015

4 Results

As the age model and some raw data have already been shown in previous publications (Zumaque et al., 2012; Caulle et al., 2013), all data will be here presented and discussed in age.

4.1 Micropaleontological assemblages characteristics

Seven taxa of planktonic foraminifera were identified in the studied section. Their concentrations vary from 0 to 2500 individuals g^{-1} of dry sediment, with a mean value of around 400, and highest values recorded during GIS (Fig. 2c). Assemblages are clearly dominated by the polar taxon *Neogloboquadrina pachyderma* s. (relative abundance ranging from 20 to nearly 100 %, Fig. 2b), peaking during GS and HS. *Globigerina bulloides*, *Turborotalita quinqueloba*, and the dextral (d) coiling form of *N. pachyderma* are major subordinate species in some intervals, in particular GIS.

In the same core section, Zumaque et al. (2012) and Caulle et al. (2013) identified more than 30 dinocyst species. Their absolute abundances are high, ranging from 800 to 90 000 cysts cm^{-3}, with a mean of 6700 cysts cm^{-3}. As for planktonic foraminifera, GIS register higher absolute abundances than GS and HS. Assemblages are diversified (Fig. 2d) and characterized by three dominant taxa (*Bitectatodinium tepikiense*, *Operculodinium centrocarpum*, and the ubiquitous *Brigantedinium* species) and three major secondary species (*Islandinium minutum*, *Pentapharsodinium dalei*, and *Nematosphaeropsis labyrinthus*). Several other species account for minor but significant percentages (see Zumaque et al., 2012; Caulle et al., 2013).

Dinocyst and foraminifera ecological indices fluctuate in phase with the abrupt climatic oscillations of the last glacial period (Fig. 2e and f). Planktonic foraminifera diversity and dominance are always negatively correlated, with low values of diversity and high values of dominance during GS and HS, and inversely during GIS. Dinocysts diversity and dominance variations are mostly opposite, with generally higher values of diversity and lower values of dominance during GS and HS compared to GIS; they

CPD
11, 2077–2119, 2015

appear covariant only along three very short intervals during the Last Glacial Maximum (LGM) around 20.7, 21.2 and 22.9 ka BP.

4.2 Sea-surface hydrological parameters

Paleohydrological conditions reconstructed on the 12–42 ka BP section of the studied core on the basis of planktonic foraminifera and dinocyst assemblages via modern analogue technique are shown in Fig. 3.

Planktonic foraminifera-derived mean summer temperatures (or mean summer F-Temp) vary between 2.5 and 10 °C, on average around 7 °C, and mean winter F-Temp range from −0.6 to 6.1 °C with a mean around 3 °C. These reconstructed F-Temp are lower than modern SST over the studied area which are around 11.7 and 8.6 °C on average for summer and winter seasons respectively (WOA09 data; Locarnini et al., 2010). Despite the gap of nearly 4 °C between these two signals, they both show similar trends with higher F-Temp during GIS and lower values during GS and HS (Fig. 3b).

Mean winter SST stemming from dinocysts display similar amplitudes of variation to those of mean winter F-Temp, but with a range from −0.7 to 7.0 °C and a mean around 1 °C. On the contrary, mean summer SST derived from dinocysts vary between 8.2 and 16.1 °C, with a mean value of 14.5 °C, and are thus largely above modern SST and very different from summer F-Temp. They also show a clear opposite trend to the three other reconstructed temperature signals since they display higher values during GS and HS. Besides, dinocyst SST (particularly February SST) variations appear gradual whereas F-Temp ones seem to be more abrupt in spite of an equal resolution (Fig. 3b).

Seasonality signals derived from dinocysts and planktonic foraminifera (calculated as mean summer minus mean winter temperatures, Fig. 3c) are clearly different from each other. The dinocyst-derived seasonality record displays large variations, with higher values during GS and the LGM (maximum of 15.1 °C, for an average of 13.6 °C) and lower ones during GIS (minimum of 5.7 °C). On the contrary, the foraminifera-derived seasonality signal does not exhibit any significant variation throughout the studied period since values vary between 2.4 and 5.1 °C with a mean value of 4.1 °C.

CPD
11, 2077–2119, 2015

SSS derived from dinocysts (Fig. 3d) show synchronous oscillations of similar amplitude during both seasons, mean winter SSS varying between 31.1 and 34.6 psu (mean of 32 psu) and mean summer SSS ranging from 29.9 to 34.2 psu (mean of 31 psu). They are lower than the modern mean annual value over the area of 35.3 psu (WOA09 data; Antonov et al., 2010), thus indicating more brackish surface waters in the area during the studied period. As dinocyst SST, dinocyst SSS show a consistent pattern during DO, with gradual increases during GIS and progressive decreases during GS. Indicative of freshwater advection in surface (Eynaud et al., 2007), coenobia of *Pediastrum* spp. are present when low dinocysts-derived SSS are recorded, i.e. during stadials (GS and HS) as well as during the LGM, and generally disappear during GIS (Fig. 3e); but their concentration describes a sensibly different MIS3 pattern with peaks of abundance at the stadial-interstadial and/or interstadial-stadial transitions.

Local $\delta^{18}O_{SW}$ signal derived from foraminifera (here used as an indicator of local salinity changes) also responded to the millennial-scale variability (Fig. 3f). Values vary between around −2 and 1 ‰, the lowest ones being recorded during HS1 and HS4 and the highest ones during GIS, the LGM and towards the Holocene.

LLG concentrations describe a general scheme rather similar to the local $\delta^{18}O_{SW}$ and F-Temp signals (Fig. 3). They are generally higher during GS and HS than during GIS. Only two noticeable exceptions exist: a high LLG concentration during the second half of GIS8, and very few LLG during most of HS3.

4.3 Deep-sea proxies

The millennial-scale variability has also been well captured by proxies related to bottom conditions as shown in Fig. 4. Compared to stadials (i.e. GS and HS), GIS are characterized by higher sedimentation rates, coarser grain-sizes, a higher proportion of the coarse silt fraction relative to the fine silt fraction, a coarser dominant fraction, higher magnetic susceptibility values, and higher benthic foraminifera concentrations. Among stadials, only HS2 exhibits a signature comparable to GIS one. Note that except for magnetic susceptibility (and sedimentation rate), all the other deep-sea proxies

CPD
11, 2077–2119, 2015

seem to increase gradually throughout GIS. It is visible for GIS 11, 10 and 7, and particularly noticeable for GIS 8; for shorter GIS, this progressive trend is hardly or not distinguishable.

5 Discussion

5.1 A reworked signal?

Considering the size of micro-organisms used in this study and the sedimentary processes occurring in the area, one could object that assemblages may not result from local deposition only but also from lateral advections including reworking of previously deposited material on proximal areas. In this case, our reconstructions would not reflect local surface and subsurface hydrology but a combination of allochthonous and autochthonous signals, furthermore mixed throughout time.

To identify and circumscribe these problems, we used the methodology preconized by Londeix et al. (2007) to identify reworked intervals in sedimentary records by combining diversity and dominance indices in microfossil communities. Indeed, according to these authors, ecologically inconsistent covariance between these two indices is attributed to mixing processes. In core MD99-2281, diversity and dominance are negatively correlated all along the 12–42 ka BP studied section regarding both planktonic foraminifera and dinocysts (except for three very short episodes during the LGM, a period not discussed in this study, and only for dinocysts, Fig. 2e and f), and so do not reveal any evidence of reworking.

5.2 Interpretation of proxies

5.2.1 Proxies of surface and subsurface hydrology

As shown in Fig. 3 and described in part 4.2, dinocyst-derived and planktonic foraminifera-derived hydrological signals share features in common but also dif-

CPD
11, 2077–2119, 2015

fer in some points through the studied period. Firstly, at stadial-interstadial transitions, dinocyst-derived SST and SSS display gradual increases/decreases whereas foraminifera-derived temperatures and local $\delta^{18}O_{SW}$ show more abrupt variations (Figs. 3b and 6a). Secondly, dinocysts mainly recorded a large seasonality with significant variations over the studied period whereas planktonic foraminifera recorded a low seasonality with very low or even nil fluctuations (Fig. 3c). These results clearly illustrates the fact that these organisms do not thrive at the same water depth, dinoflagellates inhabiting the uppermost 50 m and planktonic foraminifera living deeper (potentially between 0 and 300 m water depth considering the dominant and subordinate species of this study, see Table 3 in Staines-Urías et al. (2013) and references therein). Therefore, we can reasonably consider here that dinocysts provide a record of the surface sensu stricto, whereas planktonic foraminifera recorded hydrological conditions of a larger section of the top of the water column that we call hereafter the subsurface for simplicity. Modern seasonality values (calculated from WOA09 data as mean summer minus mean winter oceanic temperatures; Locarnini et al., 2010) over the studied area at the surface (~ 3.2 °C) and at 150 m water depth (~ 0.5 °C), even if lower than the recorded ones, tend to confirm this interpretation and suggest that during the last glacial period, the studied area experienced larger seasonality contrasts than today. Furthermore, this interpretation explains why dinocyst (i.e. surface) signals are noisier than planktonic foraminifera ones. Then, looking at the general trend of dinocyst-derived parameters (relatively low SSS and large seasonal amplitudes of SST, Fig. 3), it seems that the study area was overlaid by a thin freshwater surface layer of low thermal inertia during most of the studied period. This freshwater layer was certainly responsible for a strong stratification of the water column due to the presence of a halocline. This is also suggested qualitatively, i.e. at the scale of encountered species at that time, as the most abundant dinocyst species is *B. tepikiense*, a taxon which displays a strong affinity for stratified surface waters characterized by a large seasonality (Rochon et al., 1999).

CPD
11, 2077–2119, 2015

Iceberg calving and associated meltwater inputs are potential initiator and feeder of this halocline. Ice-rafted debris have mainly been used as tracers of these iceberg surges. Here, we use LLG concentrations and assume, as generally admitted, that LLG are mainly constituted of IRD. Our LLG signal is indeed very similar to IRD records coming from many studies and sites in North Atlantic (e.g. Bond and Lotti, 1995; Elliot et al., 1998, 2001; Van Kreveld et al., 2000; Rasmussen and Thomsen, 2004; Dickson et al., 2008) which described higher ice-rafted debris concentrations during GS and HS and variable concentrations during the LGM. This comforts the assumption that our LLG signal can be used as an indicator of iceberg delivery to the studied site. In this case, the resemblance between LLG concentrations and local $\delta^{18}O_{SW}$ and subsurface temperature (F-Temp) signals suggests that these latter signals are at least partly forced by iceberg calving and melting and associated cold freshwater releases. However, variations in the Atlantic inflow could also play a major role in the fluctuations of these signals. Many freshwater model experiments (e.g. Manabe and Stouffer, 1995; Ganopolski and Rahmstorf, 2001; Levine and Bigg, 2008) have indeed shown that these two processes are clearly linked, in the sense that (i) freshwater release weakens the Atlantic meridional overturning circulation and limits the northward extension of the NAD, and (ii) the larger the amount of released freshwater is, the more weaken the oceanic circulation is. Moreover, the correspondence between LLG and foraminifera-derived signals is only partial. Some delays (e.g. during H4, GS8, GS6) and incoherencies (e.g. the relatively long periods before and after HS2 with considerably low SSSs but almost no LLG) can indeed be noticed. This leads us to think that paleo-fluctuations of our foraminifera-derived signals are the result of the combined two phenomena: the warm and saline Atlantic water northward inflow and its southward retreat, and the episodic cold and fresh water release associated with iceberg surges. Respective contributions of these two phenomena could seem difficult to dissociate, but in this study, dinocyst data provide valuable clues. Indeed, as mentioned above, dinocyst-derived SSS and seasonality signals are indicators of surface stratification. Then we can suppose that during periods of high surface stratification (i.e.

CPD
11, 2077–2119, 2015

periods when the halocline strongly hampers or even prevents mixing between surface and subsurface waters), variations of F-Temp and local $\delta^{18}O_{SW}$ should be principally due to variations in the NAD intensity. At the opposite, during periods of weaker surface stratification, and when iceberg calving occurred, variations of planktonic foraminifera-derived parameters should be the result of the combination of meltwater inputs from the surface and NAD variations; but during periods of low stratification and without iceberg calving, subsurface hydrological variations should be due to NAD fluctuations only.

5.2.2 Proxies of deep water currents

Reconstructing past variations of the NSOW dynamics deserves to be attempted in this study as our multi-proxy approach provides various indicators of bottom current activities (Fig. 4). The first type of bottom flow proxy corresponds to parameters derived from grain-size measurements. These parameters (listed in Sect. 3.3 and below) have been widely employed in reconstructions of bottom current activity (e.g. McCave et al., 1995a, b; McCave, 2007; Bianchi and McCave, 1999; Hodell et al., 2009). Their use is based on the fact that bottom currents preferentially affect the silt fraction (10–63 µm) by size-sorting, such as stronger currents induce a coarsening and an increase of the relative proportion of this size fraction. Basically, an intensification of the NSOW will be depicted as a coarsening of D10, D50, and D90 (Fig. 4c), an increase of the mean size of the 10–63 µm fraction (Fig. 4d) and of the silt ratio (Fig. 4e), a coarsening of the dominant mode towards values corresponding to the silt fraction or even coarser (Fig. 4f), and a grain size distribution showing a coarsening and an increase of the relative proportion of this coarse fraction (Fig. 4c). It is important to note that in the glacial North Atlantic Ocean, IRD < 150 µm could constitute a potential source of silt-size particulates which could bias the use of these parameters as bottom flow proxies (Prins et al., 2002). Nevertheless, in our case, LLG concentrations are generally higher during GS, i.e. when grain-size distribution and parameters indicate a general finning of the total sediment fraction – including silt fraction – and a predominance of the < 10 µm fraction. As the supplies of IRD > 150 µm (i.e. LLG) and < 150 µm are supposed to be

CPD
11, 2077–2119, 2015

synchronous, the impact of IRD inputs (fine as well as coarse ones) on the grain-size distribution seems to be minor, and so do not seem to bias the use of grain-size parameters as indicators of the bottom current strength. In a similar way, biogenic inputs could also influence grain-size distribution and bias the grain-size proxies. However, Fig. 4d–f show that the calculated grain-size parameters for the bulk samples and for the pretreated ones exhibit the same variations in terms of timing as well as in amplitude. Grain-size analyses on pretreated samples were besides conducted on the core section where the content of $CaCO_3$ (data not shown) display the largest variations and attains its maximal value over the studied portion of the core. This confirms that in our study area, grain-size variations of bulk sediment almost exclusively reflect changes in the terrigenous fraction and so can be directly interpreted in terms of fluctuations of the bottom current intensity.

The second type of bottom flow proxy used in this study is the magnetic susceptibility (Fig. 4g). Kissel et al. (1999, 2009) have shown that, in areas distributed along the path of the deep water-masses feeding the North Atlantic Deep Water, magnetic susceptibility fluctuations are directly related to variations in the relative amount of magnetic particulates within the sediment; as those magnetic minerals principally originates from a unique source (the Nordic basaltic province), changes in magnetic susceptibility reflect changes in the efficiency of their transport mode from the source area to the study site, i.e. changes in the intensity of bottom currents. Hence, in our study area, higher values of magnetic susceptibility reflect higher NSOW energy.

Our last type of indicator of bottom flow activity corresponds to benthic foraminiferal concentrations (Fig. 4h). Indeed, in the study of two cores located northeast off Faeroes, Rasmussen et al. (1999) related this parameter to the activity of the NSOW, with high concentrations of benthic foraminifera associated with relatively strong bottom current influence and increased ventilation and supply of food, and conversely low benthic abundances related to more quiet deep-sea conditions with reduced fluxes of organic matter.

CPD
11, 2077–2119, 2015

When looking at the evolution of all these proxies in core MD99-2281, it clearly appears that they all tend to the same general scheme: the NSOW was relatively active during GIS and relatively reduced during GS (Figs. 4 and 5). This results are in accordance with findings from previous studies (e.g. Moros et al., 1997, 2002; Van Kreveld et al., 2000; Elliot et al., 2002; Rasmussen and Thomsen, 2004; Ballini et al., 2006). Besides, the higher sedimentation rates recorded during GIS (Fig. 4b) indicate that in our study area and during the studied period, the NSOW was responsible of a higher supply of sediment during episodes of high activity rather than of a winnowing of the clay fraction (< 10 µm).

One could argue that since the age model of the studied core is based on correlations between our magnetic susceptibility record and the $\delta^{18}O$ signal of NGRIP ice-core (i.e. on the assumption that the NSOW was reduced during GS), we cannot make any supposition about the timing of changes in deep current intensity. This would be obviously true in the case of studies intending to precisely compare the timing of these changes relatively to the timing of Greenland atmospheric variations. But this is not the case of our study, which aims to compare the timing of deep circulation changes with the one of surface and subsurface hydrological variations, and to compare the trends of all those fluctuations (progressive *vs.* abrupt).

5.3 Hydrological signature during Dansgaard–Oeschger events and implications

MD99-2281 records are in general agreement with the usual climatic scheme depicted in previous studies and described in the introduction of this paper, i.e. iceberg surges and a weaker or deeper Atlantic meridional overturning circulation during GS, and conversely warmer surface conditions linked to a more northerly inflow of Atlantic surface waters and associated active deep water convection in the Nordic Seas during GIS (cf. Fig. 5). This is especially noticeable with the strong and striking correlation between dinocysts, planktonic and benthic foraminifera abundances throughout all the studied

CPD
11, 2077–2119, 2015

period, which furthermore suggests a coupling of the productivity at the different layers of the water column.

However our records also reveal unusual features, such as the strong stratification of surface waters during GS. Previous studies from the subpolar North Atlantic (e.g. Rasmussen et al., 1996a, b; Rasmussen and Thomsen, 2004; Dokken et al., 2013 at study sites close to MD99-2281 site, Van Kreveld et al., 2000 in the Irminger Basin) already indirectly deduced from planktonic foraminifera data the presence of a halocline and a stratified water column during GS. In our study, dinocyst assemblages and dinocyst-derived surface hydrological parameters provide direct evidences of the presence of a thin freshwater surface layer and stratified surface waters during stadials, and therefore confirm the previous assumption based on indirect proxies (rather subsurface proxies).

Our records also show atypical progressive trends that can be depicted within GS and most of all within GIS (Figs. 3, 5 and 6a). During GS, dinocyst data indicate a deterioration of surface conditions characterized by a more or less gradual decrease of winter SST (depending on the GS considered) while summer SST, surface stratification and seasonality remain high. Foraminifera-derived subsurface hydrological parameters and grain-size data show rapid transitions at the beginning of GS (especially noticeable for GS 10 and 8 for example) which denote an abrupt slowing down of the Atlantic inflow (sharp decreases of F-Temp and local $\delta^{18}O_{SW}$) and of the deep NSOW (marked decreases in grain-sizes, silt ratio and mean size of the silt fraction) at that time. Throughout GIS, dinocyst data reveal progressively milder surface conditions marked by a gradual increase of winter SST in parallel with a gradual decrease of stratification and seasonality. Grain-size data also indicate a gradual intensification of the NSOW flow with a maximal intensity at the end of these periods (particularly noticeable when looking at the silt ratio and the mean size of the 10–63 µm fraction, and highlighted by red arrows on Fig. 5). At the opposite, planktonic foraminifera data show that the subsurface reactivation of the NAD at the GS-GIS transitions was more abrupt than shown within proxies of surface and deep-sea dynamics.

CPD
11, 2077–2119, 2015

At first sight, our set of proxies thus denotes a decoupling between surface, subsurface, and deep-sea hydrological processes during DO cycles. This is in agreement with previous studies which already suggested a decoupling between surface and subsurface (Moros et al., 2002) or subsurface and deep circulations (Rasmussen et al., 1996b). However, a scrupulous examination of our records reveals that subsurface and deep circulations are coupled during GS, i.e. when surface waters are highly stratified, and that surface and deep circulations are coupled during GIS, i.e. when the stratification is reduced. This leads us to think that the surface stratification is a determinant factor for hydrological processes occurring at greater depth around the study area. We can therefore propose the following scenario which conciliates our records and highlights the importance of the water-column organization during millennial scale climatic events (Fig. 6b):

At the end of GS, the NAD rapidly re-intensifies. However, the water column is still highly stratified and the surface halocline prevents heat exchange towards the atmosphere; heat is thus stored in the subsurface layer below the halocline. Subsurface waters are consequently not dense enough because too warm to sink and deep convection is nil or very limited. Then, at the beginning of GIS, the halocline starts to be unstable (probably because of the accumulation of heat below). The stratification is then progressively reduced, and heat exchange becomes possible again. Subsurface Atlantic waters progressively mix with low salinity surface waters which progressively get saltier. They become sufficiently dense to sink, and deep convection is thus re-activated and progressively intensifies throughout the GIS. As a consequence, the NSOW activity progressively strengthens and reaches its maximal vigor at the end of this period. Then, at the beginning of GS, iceberg discharges occur. The associated meltwater has several consequences on the stadial hydrology. First, the freshwater input rapidly propagates in the mixed surface-subsurface layer, lowers its salinity, strongly reduces deep convection, and thus weakens the NAD and the NSOW flows. Secondly, it contributes to the re-establishment of the freshwater surface layer and the associated halocline,

CPD
11, 2077–2119, 2015

and to the progressive slight strengthening of the stratification. NAD and NSOW flows remain weak until the end of GS.

Rasmussen et al. (1996a, b) and Rasmussen and Thomsen (2004) proposed a similar scenario where an accumulation of heat below the fresh surface layer is responsible for the destabilization of the halocline and the abrupt release of a large amount of heat to the atmosphere, then causing the sudden Greenland atmospheric warming. On the basis of benthic assemblages from various cores located around Faeroe Islands (e.g. ENAM93-21; 62.7383° N; −3.9987° E; 1020 m water depth – ENAM33; 61.2647° N; −11.1609° E; 1217 m water depth), they suggested that relatively warm Atlantic intermediate waters keep on flowing into the Nordic Seas below the halocline during GS, and they attributed these warm Atlantic waters to the NAD. However, our results derived from planktonic foraminifera data do not indicate any significant flow of NAD directly below the halocline during GS (Rasmussen et al., 1996a, b; Rasmussen and Thomsen, 2004 recorded indeed a total dominance of *Neogloboquadrina pachyderma* s. during stadials), but suggest such a flow at intermediate water depth, in-between the subsurface and bottom layers. In this case, both the reactivation of the subsurface NAD at the end of GS and the continuous northward flow of Atlantic intermediate waters during GS may have participated in the accumulation of heat below the halocline, the destabilization of this latter, and then the sudden release of heat to the atmosphere at the GS-GIS transition.

Dokken et al. (2013) also proposed a similar scenario for GS, with a fresh surface layer, a halocline, and an active Atlantic inflow just below it. This scenario was inferred from planktonic foraminifera data in core MD99-2284 (62.3747° N; −0.9802° E; 1500 m water depth). Considering the location of their study site close to the continental shelf edge, this shallow Atlantic inflow is not contradictory to our results which allow the presence of a narrow warm Atlantic inflow flattened against the shelf edge by the Coriolis force. Such a narrow flow would not be recorded in cores located further away from the shelf such as ours.

CPD
11, 2077–2119, 2015

The observed gradual intensification of the NSOW flow during GIS constitutes the most unusual and salient feature revealed by our data. However, a previous study from the Reykjanes Ridge (Snowball and Moros, 2003) also depicted a very similar pattern in magnetic susceptibility data and quartz to plagioclase ratio in cores LO09-18GC (58.9674° N; −30.6832° E; 1460 m water depth) and SO82-05GGC (59.1857° N; −30.9047° E; 1420 m water depth), with a progressive intensification of the Iceland–Scotland Overflow Water during GIS followed by an abrupt reduction.

5.4 Different hydrological patterns during Heinrich stadials

Figure 5 clearly shows that the four HS recorded in the studied section of core MD99-2281 (HS1, HS2, HS3 and HS4) do not exhibit the same hydrological patterns. The only common feature corresponds to the harsh surface conditions deduced from dinocyst data and also depicted during GS, and characterized by the presence of a fresh lid, a high seasonality and a relatively strong stratification of the water column. On the contrary, planktonic foraminifera data and deep-sea proxies show different signals, in amplitude or in trend, thus suggesting different subsurface and deep water mass dynamics (see Table 1).

HS1 and HS4 appear such as HS are usually described in the literature, i.e. with very low local $\delta^{18}O_{SW}$ values indicative of very low salinities in the subsurface layer, and strongly reduced or even shut down Atlantic inflow and deep-water overflow (according to foraminifera-derived data and grain-size data respectively). Compared to GS, our data indicate a more drastic reduction of the meridional overturning circulation and a more southerly location of the deep convection center during HS1 and HS4, in agreement with previous studies (e.g. Elliot et al., 2002; Rahmstorf, 2002).

At the opposite, HS2 presents a very atypical hydrological signature: grain-size data, in agreement with the magnetic susceptibility signal, indicate a relatively active NSOW; in parallel, subsurface records show F-Temp and local $\delta^{18}O_{SW}$ comparable to most of GS ones but higher than the classical HS1 and HS4 and even than some GS. These results indicate the presence of saltier (and so denser) and slightly warmer subsurface

CPD
11, 2077–2119, 2015

waters bathing our study site, and thus denotes a relatively active meridional overturning circulation and a more northerly center of convection during HS2 compared to "classical" HS. This would be besides in agreement with previous paleoreconstructions: in core Na 87-22 (located on the eastern banks of the Rockall Plateau; 55.4833° N; −14.6833° E; 2161 m water depth), Elliot et al. (2002) found benthic $\delta^{13}C$ values during HS2 which are higher than HS1 and HS4 values and similar to GS values; according to the interpretation of this proxy made by the authors, it suggests that the reduction of deep-water formation and the northward migration of $\delta^{13}C$ depleted southern source deep waters were less important during HS2 and stadials than during HS1 and HS4. Much farther away from our study area, in the Gulf of Cadiz, core MD99-2339 (35.88° N, −7.53° E; 1170 m water depth; Voelker et al., 2006) also provides indirect evidence of a more active North Atlantic overturning circulation. Indeed, paleoreconstructions of the strength of the Mediterranean Outflow Water (or MOW, which overflows from the Mediterranean Sea to and within the Gulf of Cadiz) have shown that this bottom current has been particularly active during periods of weak Atlantic meridional overturning circulation such as GS and HS (e.g. Cacho et al., 2000; Voelker et al., 2006; Toucanne et al., 2007). Grain-size data of core MD99-2339 show indeed a clear intensification of the MOW during HS1, HS4, HS5, and most GS. However they do not indicate such a strengthening during HS2 (and HS3), and so could denote a more vigorous North Atlantic circulation.

Concerning HS3, grain-size data tend to indicate a low NSOW activity throughout the event. However, foraminifera-derived subsurface parameters show a tripartite structure with (i) low F-Temp and local $\delta^{18}O_{SW}$ values indicative of a weak NAD at the beginning and the end of the event and (ii) higher values pointing to a stronger NAD in the central part of the event. Besides, the magnetic susceptibility record shows two peaks around 29.5 and 30.5 ka BP coeval with high F-Temp and local $\delta^{18}O_{SW}$ values. Furthermore, Elliot et al. (2002) found a two-phased incursion of southern sourced waters (at the onset and the termination of the event) in core Na 87-22 from the Rockall Plateau and core SU90-24 from the Irminger Basin (62.0667° N; −37.0333° E; 2100 m water depth).

CPD
11, 2077–2119, 2015

These records hence suggest that HS3 might have been a three-phased event with classical disruptions of the overturning circulation at the end and the beginning of the event interrupted by a significant resumption of this circulation. Such an intensification and associated northward migration of the NAD in the middle of HS3 might have induced additional iceberg calving from European ice-sheets and could thus explain the relatively long duration of this HS (as already advanced by Elliot et al., 2002) as well as the dominant European sources of IRD. The absence of clear evidence of such a reactivation of the NSOW in grain-size data, and its discrete and arguable evidence in the magnetic susceptibility record is puzzling if we consider, as advanced previously, that subsurface and deep circulations should be coupled due to the strong surface stratification. However, the Wyville–Thompson Ridge could have acted as a topographic barrier (as episodically today) that would have prevented a too weak deep flow to influence our study site by constraining it into the Faeroe Bank Channel (cf. Fig. 1).

6 Conclusions

Analyses carried out within the framework of this study confirm that the area southwest off Faeroe Islands has been very sensitive to the last glacial millennial-scale climatic variability. Our multiproxy approach allows us to track hydrological processes at different key water depths, and reveals a partly and episodically coupling of surface, subsurface and deep water mass dynamics controlled by surface stratification during rapid climatic shifts. Indeed, GIS are characterized by a decreasing stratification and a coupling of surface and deep hydrological processes, with progressively milder surface conditions and gradual intensification of the NSOW while the activity of the subsurface NAD inflow remains constantly high. At the opposite, GS experienced a high surface stratification and coupled subsurface and deep circulations marked by a sharp weakening of the NAD and the NSOW at the beginning of GS, while surface conditions progressively deteriorate throughout the GS. These results led us to propose a scenario describing the evolution and interactions of hydrological processes during DO cycles and taking

CPD
11, 2077–2119, 2015

into account the determining role of the surface stratification. Our records also denote different hydrological signatures during Heinrich stadials. HS1 and HS4 appear as "classical" HS with strongly reduced Atlantic meridional overturning circulation. On the contrary, HS2 probably experienced a relatively active North Atlantic circulation. Finally, HS3 seems to be a three-phased event marked by a re-intensification of the overturning circulation in the middle of the event.

Our study highlights the importance of dinocysts as a proxy of oceanic surface sensu stricto conditions in subpolar environments during, at least, the last glacial period. It illustrates the potential of such high resolution multi-proxy paleoreconstructions, especially in areas close to glacial ice-sheets when aiming to track hydrological processes occurring during the still so enigmatic rapid climatic oscillations of glacial periods. It also encourages model experiments to take into account stratification artifacts and 3-D-oceanic scenarios, and to test the robustness of the hydrological mechanisms and interactions proposed in this work.

Acknowledgements. Part of the analyses conducted on MD99-2281 was supported by the *French INSU (Institut National des Sciences de l'Univers) program LEFE* (Les enveloppes fluides et l'environnement) within the frame of the *EVE (Evolution et variabilité du climat à l'échelle globale)* 2009–2011 project "RISCC: Rôle des Ice-Shelves dans le Changement Climatique" and of the *IMAGO (Interactions multiples dans l'atmosphère, la glace et l'océan)* 2013 project "ICE-BIO-RAM: Impact des Changements Environnementaux sur la BIOdiversité marine lors des Réchauffements Abrupts du cliMat". We also acknowledge financial support by the ARTEMIS ^{14}C AMS French project. This is Past4Future contribution no XX. The research leading to these results has received funding from the *European Union's Seventh Framework programme* (FP7/2007–2013) under grant agreement no 243908, "Past4Future. Climate change – Learning from the past climate".

We thank M.-H. Castera, I. Billy, P. Lebleu, O. Ther, M. Georget for invaluable technical assistance at EPOC laboratory. We also warmly thank L. Londeix, D. Swingedouw and M. Cremer for their precious advice and enriching discussions which contributed to greatly improve the present study. Data provided in this paper can be obtained through written request to M. Wary.

This is an U.M.R. EPOC 5805 (Université de Bordeaux – C.N.R.S.) contribution.

CPD
11, 2077–2119, 2015

References

Alvarez-Solas, J., Charbit, S., Ritz, C., Paillard, D., Ramstein, G., and Dumas, C.: Links between ocean temperature and iceberg discharge during Heinrich Events, Nat. Geosci., 3, 122–126, 2010.

Andersen, K. K., Svensson, A., Johnsen, S. J., Rasmussen, S. O., Bigler, M., Röthlisberger, R., Ruth, U., Siggaard-Andersen, M. L., Peder Steffensen, J., Dahl-Jensen, D., Vinther, B. M., and Clausen, H. B.: The Greenland ice core chronology 2005, 15–42 ka. Part 1: Constructing the time scale, Quaternary Sci. Rev., 25, 3246–3257, 2006.

Antonov, J. I., Seidov, D., Boyer, T. P., Locarnini, R. A., Mishonov, A. V., Garcia, H. E., Baranova, O. K., Zweng, M. M., and Johnson, D. R.: World Ocean Atlas 2009, Volume 2: Salinity, edited by: Levitus, S., NOAA Atlas NESDIS 69, U.S. Government Printing Office, Washington, D.C., 184 pp., 2010.

Ballini, M., Kissel, C., Colin, C., and Richter, T.: Deep-water mass source and dynamic associated with rapid climatic variations during the last glacial stage in the North Atlantic: a multiproxy investigation of the detrital fraction of deep-sea sediments, Geochem. Geophy. Geosy., 7, Q02N01, doi:10.1029/2005GC001070, 2006.

Bianchi, G. G. and McCave, I. N.: Holocene periodicity in North Atlantic climate and deep-ocean flow south of Iceland, Nature, 397, 515–517, 1999.

Boldreel, L. O., Andersen, M. S., and Kuijpers, A.: Neogene seismic facies and deep-water gateways in the Faeroe Bank area, NE Atlantic, Mar. Geol., 152, 129–140, 1998.

Bond, G., Broecker, W., Johnsen, S., McManus, J., Labeyrie, L., Jouzel, J., and Bonani, G.: Correlations between climate records from North Atlantic sediments and Greenland ice, Nature, 365, 143–147, 1993.

Bond, G. C. and Lotti, R.: Iceberg discharges into the North Atlantic on millennial time scales during the last glaciation, Science, 267, 1005–1010, 1995.

Cacho, I., Grimalt, J. O., Sierro, F. J., Shackleton, N., and Canals, M.: Evidence for enhanced Mediterranean thermohaline circulation during rapid climatic coolings, Earth Planet. Sc. Lett., 183, 417–429, 2000.

Caley, T. and Roche, D. M.: δ^{18}O water isotope in the *i*LOVECLIM model (version 1.0) – Part 3: A palaeo-perspective based on present-day data–model comparison for oxygen stable isotopes in carbonates, Geosci. Model Dev., 6, 1505–1516, doi:10.5194/gmd-6-1505-2013, 2013.

CPD
11, 2077–2119, 2015

Caulle, C., Penaud, A., Eynaud, F., Zaragosi, S., Roche, D. M., Michel, E., Boulay, S., and Richter, T.: Sea-surface hydrographical conditions off south Faeroes and within the north-eastern North Atlantic through MIS 2: the response of dinocysts, J. Quaternary Sci., 28, 217–228, 2013.

Dansgaard, W., Johnsen, S. J., Clausen, H. B., Dahl-Jensen, D., Gundestrup, N. S., Hammer, C. U., Hvidberg, C. S., Steffensen, J. P., Sveinbjörnsdottir, A. E., Jouzel, J., and Bond, G.: Evidence for general instability of past climate from a 250-kyr ice-core record, Nature, 364, 218–220, 1993.

Dickson, A. J., Austin, W. E. N., Hall, I. R., Maslin, M. A., and Kucera, M.: Centennial-scale evolution of Dansgaard–Oeschger events in the northeast Atlantic Ocean between 39.5 and 56.5 ka BP, Paleoceanography, 23, PA3206, doi:10.1029/2008PA001595, 2008.

Dokken, T. M., Nisancioglu, K. H., Li, C., Battisti, D. S., and Kissel, C.: Dansgaard–Oeschger cycles: interactions between ocean and sea ice intrinsic to the nordic seas, Paleoceanography, 28, 491–502, 2013.

Duplessy, J. C., Labeyrie, L., Juillet-Leclerc, A., Maitre, F., Duprat, J., and Sarnthein, M.: Surface salinity reconstruction of the North Atlantic Ocean during the Last Glacial Maximum, Oceanol. Acta, 14, 311–324, 1991.

Ehlers, J. and Gibbard, P. L.: The extent and chronology of Cenozoic Global Glaciation, Quatern. Int., 164–165, 6–20, 2007.

Elliot, M., Labeyrie, L., Bond, G., Cortijo, E., Turon, J. L., Tisnerat, N., and Duplessy, J. C.: Millennial-scale iceberg discharges in the Irminger Basin during the last glacial period: relationship with the Heinrich Events and environmental settings, Paleoceanography, 13, 433–446, 1998.

Elliot, M., Labeyrie, L., Dokken, T., and Manthe, S.: Coherent patterns of ice-rafted debris deposits in the nordic regions during the last glacial (10–60 ka), Earth Planet. Sc. Lett., 194, 151–163, 2001.

Elliot, M., Labeyrie, L., and Duplessy, J. C.: Changes in North Atlantic deep-water formation associated with the Dansgaard–Oeschger temperature oscillations (60–10 ka), Quaternary Sci. Rev., 21, 1153–1165, 2002.

Epstein, S. and Mayeda, T.: Variation of O^{18} content of waters from natural sources, Geochim. Cosmochim. Ac., 4, 213–224, 1953.

CPD
11, 2077–2119, 2015

Eynaud, F., Turon, J. L., Matthiessen, J., Kissel, C., Peypouquet, J. P., De Vernal, A., and Henry, M.: Norwegian sea-surface palaeoenvironments of marine oxygen-isotope stage 3: the paradoxical response of dinoflagellate cysts, J. Quaternary Sci., 17, 349–359, 2002.

Eynaud, F., Zaragosi, S., Scourse, J. D., Mojtahid, M., Bourillet, J. F., Hall, I. R., Penaud, A., Locascio, M., and Reijonen, A.: Deglacial laminated facies on the NW European continental margin: the hydrographic significance of British–Irish Ice Sheet deglaciation and Fleuve Manche paleoriver discharges, Geochem. Geophy. Geosy., 8, Q06019, doi:10.1029/2006GC001496, 2007.

Eynaud, F., Rossignol, L., and Gasparotto, M.-C.: Planktic foraminifera throughout the Pleistocene: from cell to populations to past marine hydrology, in Foraminifera: Classification, Biology, and Evolutionary Significance, edited by: Georgescu, M. D., Nova Science Publishers, New York, NY, 2013.

Ganopolski, A. and Rahmstorf, S.: Rapid changes of glacial climate simulated in a coupled climate model, Nature, 409, 153–158, 2001.

Goodman, D. K.: Dinoflagellate "communities"; from the lower Eocene Nanjemoy formation of Maryland, U.S.A, Palynology, 3, 169–190, 1979.

Guiot, J. and de Vernal, A.: Transfer functions: methods for quantitative paleoceanography based on microfossils, Chapt. thirteen, in: Developments in Marine Geology, edited by: Hillaire-Marcel, C. and De Vernal, A., Elsevier, 1, 523–563, 2007.

Guiot, J. and de Vernal, A.: Is spatial autocorrelation introducing biases in the apparent accuracy of paleoclimatic reconstructions?, Quaternary Sci. Rev., 30, 1965–1972, 2011a.

Guiot, J. and de Vernal, A.: QSR correspondence "Is spatial autocorrelation introducing biases in the apparent accuracy of palaeoclimatic reconstructions?", Reply to Telford and Birks, Quaternary Sci. Rev., 30, 3214–3216, 2011b.

Hansen, B. and Osterhus, S.: North Atlantic–Nordic Sea exchanges, Prog. Oceanogr., 45, 109–208, 2000.

Heinrich, H.: Origin and consequences of cyclic ice rafting in the Northeast Atlantic Ocean during the past 130,000 years, Quaternary Res., 29, 142–152, 1988.

Hodell, D. A., Minth, E. K., Curtis, J. H., McCave, I. N., Hall, I. R., Channell, J. E. T., and Xuan, C.: Surface and deep-water hydrography on Gardar Drift (Iceland Basin) during the last interglacial period, Earth Planet. Sc. Lett., 288, 10–19, 2009.

CPD
11, 2077–2119, 2015

Howe, J. A., Stoker, M. S., Masson, D. G., Pudsey, C. J., Morris, P., Larter, R. D., and Bulat, J.: Seabed morphology and the bottom-current pathways around Rosemary Bank seamount, northern Rockall Trough, North Atlantic, Mar. Petrol. Geol., 23, 165–181, 2006.

Kissel, C., Laj, C., Labeyrie, L., Dokken, T., Voelker, A., and Blamart, D.: Rapid climatic variations during marine isotopic stage 3: magnetic analysis of sediments from Nordic Seas and North Atlantic, Earth Planet. Sc. Lett., 171, 489–502, 1999.

Kissel, C., Laj, C., Piotrowski, A. M., Goldstein, S. L., and Hemming, S. R.: Millennial-scale propagation of Atlantic deep waters to the glacial Southern Ocean, Paleoceanography, 23, PA2102, doi:10.1029/2008PA001624, 2008.

Kissel, C., Laj, C., Mulder, T., Wandres, C., and Cremer, M.: The magnetic fraction: a tracer of deep water circulation in the North Atlantic, Earth Planet. Sc. Lett., 288, 444–454, 2009.

Kuijpers, A., Andersen, M. S., Kenyon, N. H., Kunzendorf, H., and Van Weering, T. C. E.: Quaternary sedimentation and Norwegian Sea overflow pathways around Bill Bailey Bank, northeastern Atlantic, Mar. Geol., 152, 101–127, 1998a.

Kuijpers, A., Troelstra, S. R., Wisse, M., Nielsen, S. H., and Van Weering, T. C. E.: Norwegian Sea overflow variability and NE Atlantic surface hydrography during the past 150,000 years, Mar. Geol., 152, 75–99, 1998b.

Kuijpers, A., Hansen, B., Hühnerbach, V., Larsen, B., Nielsen, T., and Werner, F.: Norwegian Sea overflow through the Faroe–Shetland gateway as documented by its bedforms, Mar. Geol., 188, 147–164, 2002.

Labeyrie, L. and Cortijo, E.: Physical Properties of Sediment Core MD99-2281, doi:doi:10.1594/PANGAEA.253612, 2005.

Labeyrie, L., Cortijo, E., and Jansen, E.: Rapport Scientifique de la Mission INTERPOLE MD99-114/812 IMAGES V, in: Les Rapports de Campagne à la Mer à bord du Marion Dufresne, (IPEV, Ed.), Brest, 1999.

Laj, C., Kissel, C., Mazaud, A., Channell, J. E. T., and Beer, J.: North Atlantic palaeointensity stack since 75 ka (NAPIS-75) and the duration of the Laschamp event, Philos. T. R. Soc. A, 358, 1009–1025, 2000.

Levine, R. C. and Bigg, G. R.: Sensitivity of the glacial ocean to Heinrich Events from different iceberg sources, as modeled by a coupled atmosphere-iceberg-ocean model, Paleoceanography, 23, PA4213, doi:10.1029/2008PA001613, 2008.

Locarnini, R. A., Mishonov, A. V., Antonov, J. I., Boyer, T. P., Garcia, H. E., Baranova, O. K., Zweng, M. M., and Johnson, D. R.: World Ocean Atlas 2009, Volume 1: Temperature, edited

CPD
11, 2077–2119, 2015

by : Levitus, S., NOAA Atlas NESDIS 68, U.S. Government Printing Office, Washington, D.C., 184 pp., , 2010.
Londeix, L., Benzakour, M., Suc, J. P., and Turon, J. L.: Messinian palaeoenvironments and hydrology in Sicily (Italy): the dinoflagellate cyst record, Geobios, 40, 233–250, 2007.
Malaizé, B. and Caley, T.: Sea surface salinity reconstruction as seen with foraminifera shells: methods and cases studies, Eur. Phys. J., 1, 177–188, 2009.
Manabe, S. and Stouffer, R. J.: Simulation of abrupt climate change induced by freshwater input to the North Atlantic Ocean, Nature, 378, 165–167, 1995.
McCave, I. N.: Deep-sea sediment deposits and properties controlled by currents, Chapt. One, in: Developments in Marine Geology, edited by: Hillaire-Marcel, C. and De Vernal, A., Elsevier, 1, 19–62, 2007.
McCave, I. N., Manighetti, B., and Beveridge, N. A. S.: Circulation in the glacial North Atlantic inferred from grain-size measurements, Nature, 374, 149–152, 1995a.
McCave, I. N., Manighetti, B., and Robinson, S. G.: Sortable silt and fine sediment size/composition slicing: parameters for palaeocurrent speed and palaeoceanography, Paleoceanography, 10, 593–610, 1995b.
Menviel, L., Timmermann, A., Friedrich, T., and England, M. H.: Hindcasting the continuum of Dansgaard–Oeschger variability: mechanisms, patterns and timing, Clim. Past, 10, 63–77, doi:10.5194/cp-10-63-2014, 2014.
Moros, M., Endler, R., Lackschewitz, K. S., Wallrabe-Adams, H. J., Mienert, J., and Lemke, W.: Physical properties of Reykjanes Ridge sediments and their linkage to high-resolution Greenland Ice Sheet Project 2 ice core data, Paleoceanography, 12, 687–695, 1997.
Moros, M., Kuijpers, A., Snowball, I., Lassen, S., Bäckström, D., Gingele, F., and McManus, J.: Were glacial iceberg surges in the North Atlantic triggered by climatic warming?, Mar. Geol., 192, 393–417, 2002.
Orvik, K. A. and Niiler, P.: Major pathways of Atlantic water in the northern North Atlantic and Nordic Seas toward Arctic, Geophys. Res. Lett., 29, 2–1, 2002.
Prins, M. A., Bouwer, L. M., Beets, C. J., Troelstra, S. R., Weltje, G. J., Kruk, R. W., Kuijpers, A., and Vroon, P. Z.: Ocean circulation and iceberg discharge in the glacial North Atlantic: inferences from unmixing of sediment size distributions, Geology, 30, 555–558, 2002.
Rahmstorf, S.: Ocean circulation and climate during the past 120,000 years, Nature, 419, 207–214, 2002.

CPD
11, 2077–2119, 2015

Rasmussen, T. L. and Thomsen, E.: The role of the North Atlantic Drift in the millennial timescale glacial climate fluctuations, Palaeogeogr. Palaeocl., 210, 101–116, 2004.
Rasmussen, T. L. and Thomsen, E.: Warm Atlantic surface water inflow to the Nordic seas 34–10 calibrated ka BP, Paleoceanography, 23, 2008.
Rasmussen, T. L. and Thomsen, E.: Ventilation changes in intermediate water on millennial time scales in the SE Nordic seas, 65–14 kyr BP, Geophys. Res. Lett., 36, L01601, doi:10.1029/2008GL036563, 2009.
Rasmussen, T. L., Thomsen, E., Labeyrie, L., and Van Weering, T. C. E.: Circulation changes in the Faeroe–Shetland Channel correlating with cold events during the last glacial period (58–10 ka), Geology, 24, 937–940, 1996a.
Rasmussen, T. L., Thomsen, E., Van Weering, T. C. E., and Labeyrie, L.: Rapid changes in surface and deep water conditions at the Faeroe Margin during the last 58,000 years, Paleoceanography, 11, 757–771, 1996b.
Rasmussen, T. L., Van Weering, T. C. E., and Labeyrie, L.: High resolution stratigraphy of the Faeroe–Shetland Channel and its relation to North Atlantic paleoceanography: the last 87 kyr, Mar. Geol., 131, 75–88, 1996c.
Rasmussen, T. L., Balbon, E., Thomsen, E., Labeyrie, L., and Van Weering, T. C. E.: Climate records and changes in deep outflow from the Norwegian Sea ~ 150–55 ka, Terra Nova, 11, 61–66, 1999.
Rasmussen, T. L., Thomsen, E., Troelstra, S. R., Kuijpers, A., and Prins, M. A.: Millennial-scale glacial variability versus Holocene stability: changes in planktic and benthic foraminifera faunas and ocean circulation in the North Atlantic during the last 60 000 years, Mar. Micropaleontol., 47, 143–176, 2002a.
Rasmussen, T. L., Bäckström, D., Heinemeier, J., Klitgaard-Kristensen, D., Knutz, P. C., Kuijpers, A., Lassen, S., Thomsen, E., Troelstra, S. R., and Van Weering, T. C. E.: The Faroe–Shetland Gateway: late Quaternary water mass exchange between the Nordic seas and the northeastern Atlantic, Mar. Geol., 188, 165–192, 2002b.
Rochon, A., de Vernal, A., Turon, J.-L., Matthiessen, J., and Head, M. J. (Eds.): Distribution of Dinoflagellate Cysts in Surface Sediments from the North Atlantic Ocean and Adjacent Basins and Quantitative Reconstruction of Sea-Surface Parameters, AASP special pub., Dallas, Texas, 1999.
Schlitzer, R.: Ocean Data View, available at: http://odv.awi.de (last access: 8 April 2014), 2012.

CPD
11, 2077–2119, 2015

Scourse, J. D., Haapaniemi, A. I., Colmenero-Hidalgo, E., Peck, V. L., Hall, I. R., Austin, W. E. N., Knutz, P. C., and Zahn, R.: Growth, dynamics and deglaciation of the last British–Irish ice sheet: the deep-sea ice-rafted detritus record, Quaternary Sci. Rev., 28, 3066–3084, 2009.

Shackleton, N. J.: Attainment of isotopic equilibrium between ocean water and the benthic foraminifera genus Uvigerina: isotopic changes in the ocean during the Last Glacial, in: Methodes Quantitatives d'Étude des Variations du Climat au Cours du Pleistocène, edited by: Labeyrie, L., Colloques Internationaux du CNRS, no. 219, Paris, 203–209, 1974.

Shannon, C. E. and Weaver, W.: The Mathematical Theory of Information, University of Illinois Press, Urbana, 1949.

Siddall, M., Rohling, E. J., Thompson, W. G., and Waellbroeck, C.: Marine isotope stage 3 sea level fluctuations: data synthesis and new outlook, Rev. Geophys., 46, RG4003, doi:10.1029/2007RG000226, 2008.

Snowball, I. and Moros, M.: Saw-tooth pattern of North Atlantic current speed during Dansgaard–Oeschger cycles revealed by the magnetic grain size of Reykjanes Ridge sediments at 59° N, Paleoceanography, 18, 4–1, 2003.

Staines-Urías, F., Kuijpers, A., and Korte, C.: Evolution of subpolar North Atlantic surface circulation since the early Holocene inferred from planktic foraminifera faunal and stable isotope records, Quaternary Sci. Rev., 76, 66–81, 2013.

Stanford, J. D., Rohling, E. J., Bacon, S., and Holliday, N. P.: A review of the deep and surface currents around Eirik Drift, south of Greenland: comparison of the past with the present, Global Planet. Change, 79, 244–254, 2011.

Svensson, A., Andersen, K. K., Bigler, M., Clausen, H. B., Dahl-Jensen, D., Davies, S. M., Johnsen, S. J., Muscheler, R., Parrenin, F., Rasmussen, S. O., Röthlisberger, R., Seierstad, I., Steffensen, J. P., and Vinther, B. M.: A 60 000 year Greenland stratigraphic ice core chronology, Clim. Past, 4, 47–57, doi:10.5194/cp-4-47-2008, 2008.

Toucanne, S., Mulder, T., Schönfeld, J., Hanquiez, V., Gonthier, E., Duprat, J., Cremer, M., and Zaragosi, S.: Contourites of the Gulf of Cadiz: a high-resolution record of the paleocirculation of the Mediterranean outflow water during the last 50,000 years, Palaeogeogr. Palaeocl., 246, 354–366, 2007.

Van Kreveld, S., Sarnthein, M., Erlenkeuser, H., Grootes, P., Jung, S., Nadeau, M. J., Pflaumann, U., and Voelker, A.: Potential links between surging ice sheets, circulation changes, and the Dansgaard–Oeschger cycles in the Irmiger Sea, 60–80 kyr, Paleoceanography, 15, 425–442, 2000.

CPD
11, 2077–2119, 2015

Voelker, A. H. L., Lebreiro, S. M., Schönfeld, J., Cacho, I., Erlenkeuser, H., and Abrantes, F.: Mediterranean outflow strengthening during Northern Hemisphere coolings: a salt source for the glacial Atlantic?, Earth Planet. Sc. Lett., 245, 39–55, 2006.

Waelbroeck, C., Labeyrie, L., Michel, E., Duplessy, J. C., McManus, J. F., Lambeck, K., Balbon, E., and Labracherie, M.: Sea-level and deep water temperature changes derived from benthic foraminifera isotopic records, Quaternary Sci. Rev., 21, 295–305, 2002.

Wolff, E. W., Chappellaz, J., Blunier, T., Rasmussen, S. O., and Svensson, A.: Millennial-scale variability during the last glacial: the ice core record, Quaternary Sci. Rev., 29, 2828–2838, 2010.

Zumaque, J., Eynaud, F., Zaragosi, S., Marret, F., Matsuzaki, K. M., Kissel, C., Roche, D. M., Malaizé, B., Michel, E., Billy, I., Richter, T., and Palis, E.: An ocean–ice coupled response during the last glacial: a view from a marine isotopic stage 3 record south of the Faeroe Shetland Gateway, Clim. Past, 8, 1997–2017, doi:10.5194/cp-8-1997-2012, 2012.

CPD
11, 2077–2119, 2015

Table 1. Synthesis of the main hydrologic features depicted at the study site during Heinrich stadials (HS) 1 to 4.

Event	Bottom (NSOW)	Subsurface (NAD)	Surface	Interpretations
HS1 and HS4	Weak or stopped	Weak or stopped	High stratification – No mixing between surface and subsurface waters	As usually described HS
HS2	Relatively active	More active than during HS1 and HS4		"atypical" HS Relatively active overturning circulation, center of deep convection located more northerly
HS3	Three-phased or weak	Three-phased (↓↑↓)		"three-phased event"

CPD
11, 2077–2119, 2015

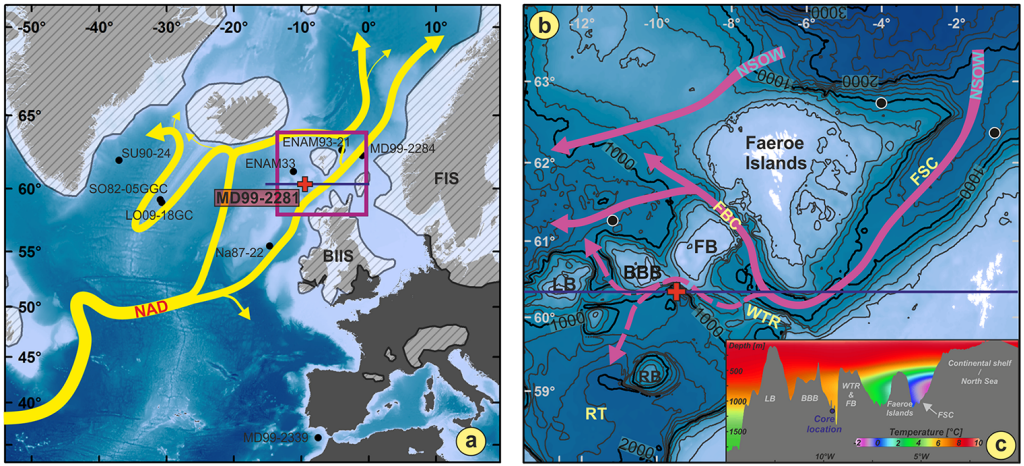

CPD
11, 2077–2119, 2015

Stratification of surface waters during the last glacial millennial climatic events

M. Wary et al.

CC BY

Figure 1. (a) General map of the studied area, showing the location of the studied core MD99-2281 (red cross) and of nearby cores referred to in the present study (black dots; ENAM93-21 and ENAM33, Rasmussen et al., 1996a, b; Rasmussen and Thomsen, 2004; MD99-2284, Dokken et al., 2013; LO09-18GC and SO82-05GGC, Snowball and Moros, 2003; Na87-22 and SU90-24, Elliot et al., 2002). The hatched areas represent the maximal last glacial extension of the proximal ice-sheets (after Ehlers and Gibbard, 2007; FIS: Fennoscandian Ice-Sheet; BIIS: British–Irish Ice-Sheet). The yellow arrows indicate the major pathways of the warm and saline surface water conveyed by the North Atlantic Drift (NAD, after Orvik and Niiler, 2002; Stanford et al., 2011). Purple square indicates the area shown in Fig. 1b. Blue line indicates the location of the profile shown in Fig. 1c. **(b)** Detailed physiography of the studied area. Bathymetry is from GEBCO (www.gebco.net, isobaths every 200 m). Remarkable sub-marine structures are indicated (bathymetric heights: FB, Faeroe Bank; BBB, Bill Bailey Bank; LB, Lousy Bank; WTR, Wyville–Thompson Ridge – trough: RT, Rockall Trough – and channels: FSC, Faeroe–Shetland Channel; FBC, Faeroe Bank Channel). Purple arrows show the major (full lines) and intermittent (dotted lines) deep Norwegian Sea Overflow Water (NSOW) pathways, after Boldreel et al., (1998), Kuijpers et al. (1998b, 2002), and Howe et al. (2006). Blue line indicates the location of the profile shown in Fig. 1c. **(c)** East–west profile of oceanic temperatures. Temperature data are derived from WOA09 (Locarnini et al., 2010) and plot using Ocean Data View (Schlitzer, 2012); bathymetric data are from GEBCO (www.gebco.net). Locations of the studied core and of the main sub-marine structures are indicated. Geographic coordinate system: WGS 1984 – Projection: Mercator 55° N.

CPD
11, 2077–2119, 2015

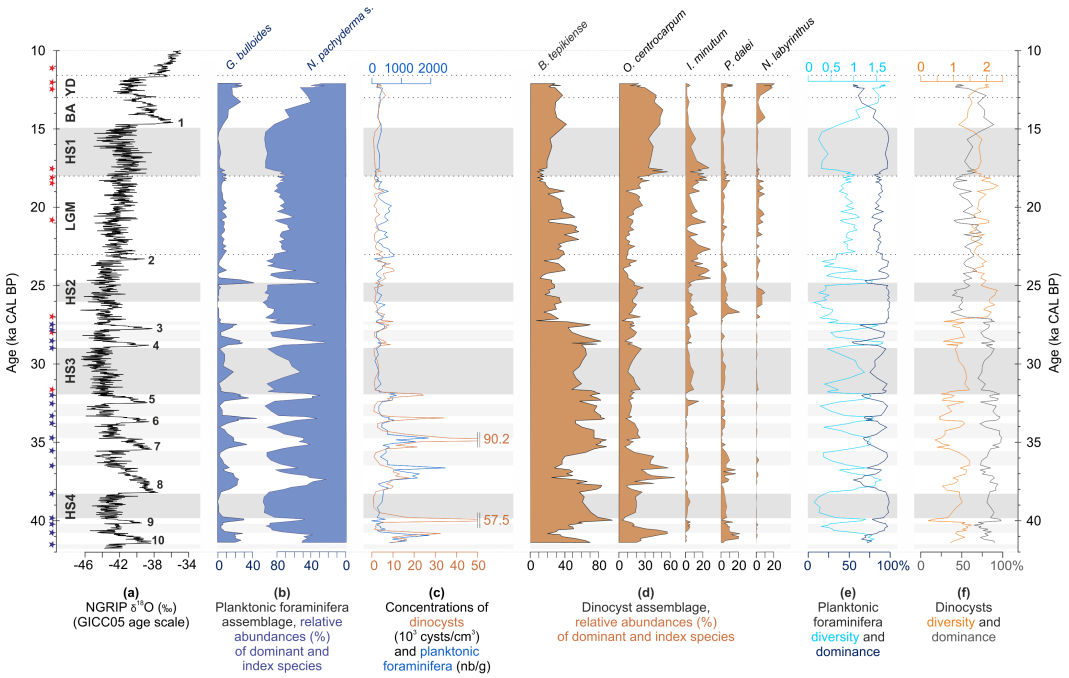

Figure 2. Evolution of index micro-planktonic assemblages compared to **(a)** NGRIP-GICC05 δ^{18}O record: – **(b)** relative abundances of the dominant planktonic foraminifera species – **(c)** absolute abundances (nb. of specimen in the sediment) of dinocysts and planktonic foraminifera – **(d)** relative abundances of dominant dinocyst species – **(e)** planktonic foraminifera diversity and dominance (see calculations in Sect. 3.2.) – **(f)** dinocyst diversity and dominance. Red stars indicate AMS ^{14}C dates used, and blue stars show the tie-points obtained by comparing the MD99-2281 magnetic susceptibility record to the NGRIP δ^{18}O signal (see Zumaque et al., 2012). GS and HS are highlighted by light and dark grey bands respectively (age limits after Wolff et al., 2010).

CPD
11, 2077–2119, 2015

Stratification of surface waters during the last glacial millennial climatic events

M. Wary et al.

CC BY

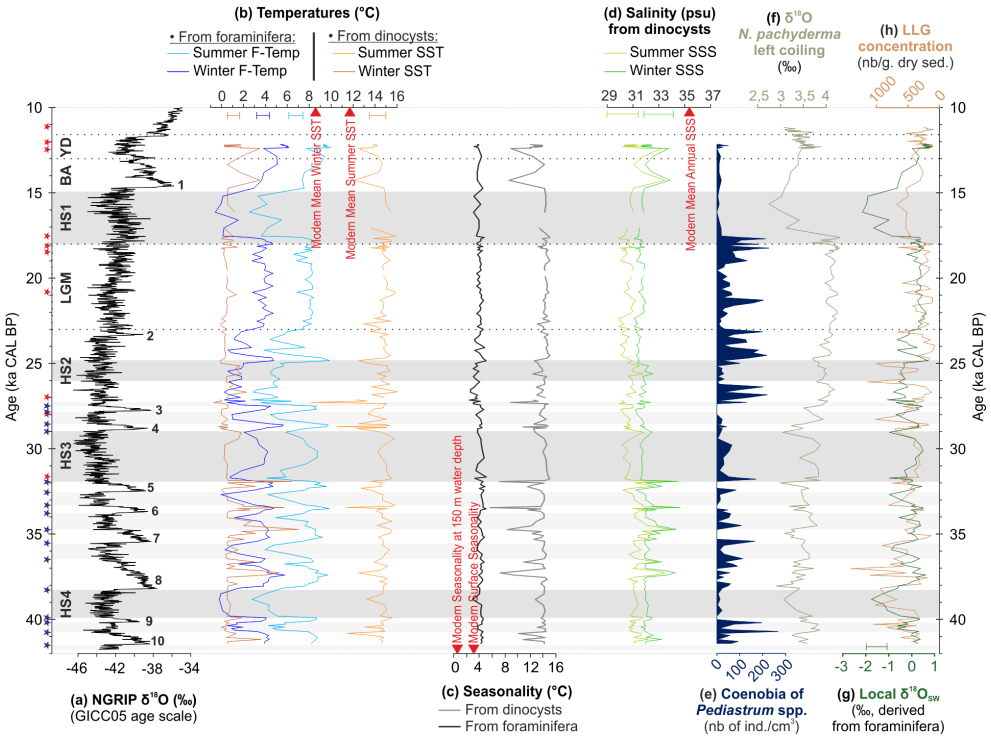

Figure 3. Reconstructed hydrological parameters derived from dinocyst and planktonic foraminifera assemblages compared to **(a)** NGRIP-GICC05 $\delta^{18}O$ record: – **(b)** temperatures – **(c)** seasonality (mean summer minus mean winter temperatures) – **(d)** SSS derived from dinocysts – **(e)** abundances of coenobia of the freshwater algae *Pediastrum* spp. – **(f)** $\delta^{18}O$ measured on *N. pachyderma* s. – **(g)** Local $\delta^{18}O_{SW}$ derived from $\delta^{18}O$ on *N. pachyderma* s. – **(h)** Large Lithic Grains – LLG concentration. Stars and bands: same legend as Fig. 2.

CPD
11, 2077–2119, 2015

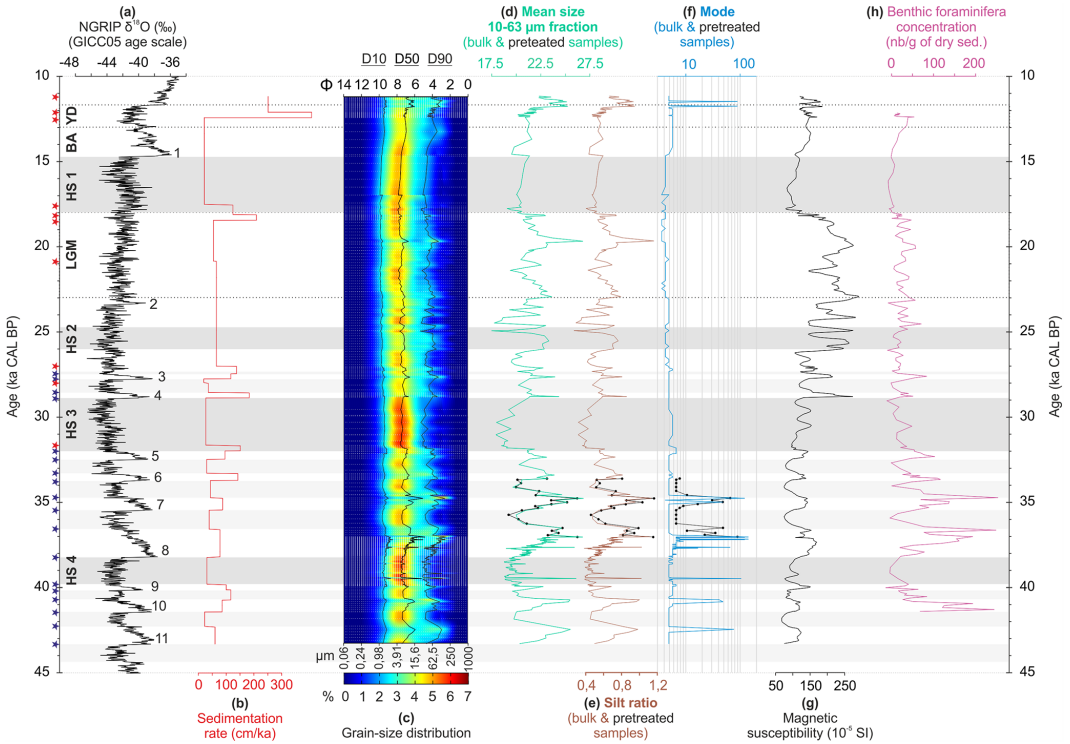

Figure 4. Evolution of oceanic bottom conditions. **(a)** NGRIP-GICC05 δ^{18}O record – **(b)** sedimentation rate (calculated between two consecutive tie-points) – **(c)** grain-size distribution on the background, and D10, D50, and D90 represented as black curves in the foreground – **(d)** mean size of the silt (10–63 µm) fraction for bulk samples and pretreated samples (carbonates and organic matter removed) – **(e)** silt ratio between 26–63 µm and 10–26 µm fractions for bulk and pretreated samples – **(f)** mean diameter of the dominant grain-size mode for bulk and pretreated samples – **(g)** magnetic susceptibility record – **(h)** absolute abundances of benthic foraminifera. Stars and bands: same legend as Fig. 2.

CPD
11, 2077–2119, 2015

Stratification of surface waters during the last glacial millennial climatic events

M. Wary et al.

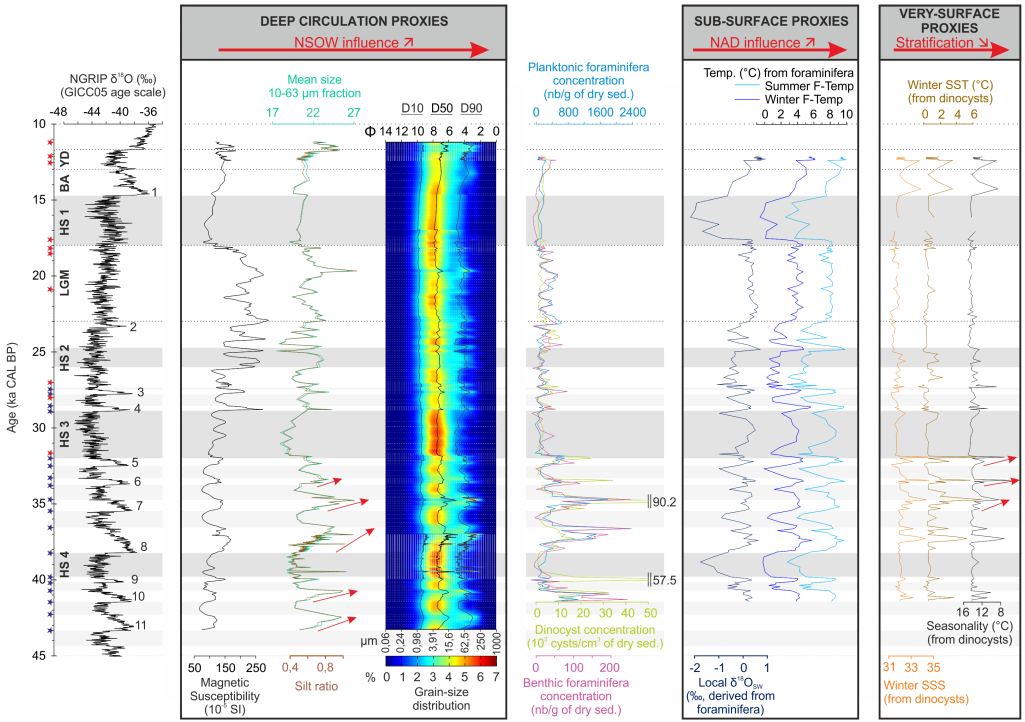

Figure 5. Comparative figure showing the evolution through time of proxies indicative of the NSOW bottom dynamics (left framed panel), the subsurface NAD intensity (middle framed panel), and the surface sensu stricto conditions (right framed panel). Absolute abundances of benthic foraminifera, planktonic foraminifera, and dinocysts are shown in the middle unframed panel. NGRIP $\delta^{18}O$ record is shown at the far left to illustrate the chronological framework. Stars and bands: same legend as Fig. 2. Red arrows highlight the progressive trends.

CPD
11, 2077–2119, 2015

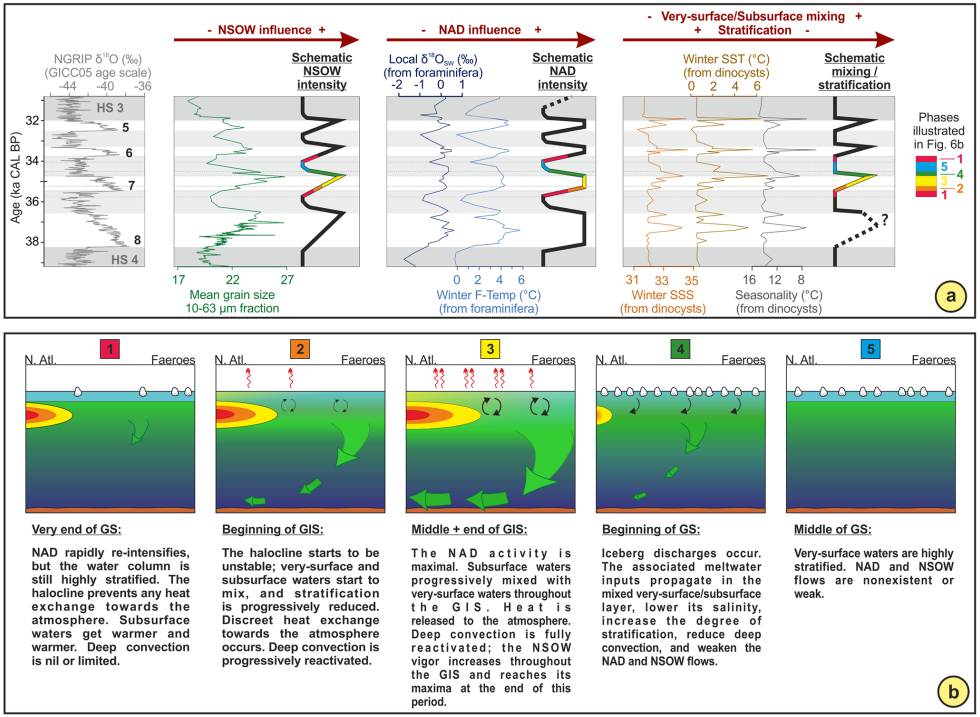

Figure 6. Synthetic figure illustrating the hydrological processes occurring during Dansgaard–Oeschger cycles at the study site. **(a)** Zoom in on DO 8, 7, 6 and 5 showing the evolution of some selected proxies shown in Fig. 5, as well as the schematic evolution through DO cycles of the NSOW activity, the NAD vigor, the intensity of mixing between surface and subsurface waters, and the degree of surface stratification. **(b)** Conceptual representation of the hydrological processes occurring during the different phases within DO cycles depicted in Fig. 6a.

CPD
11, 2077–2119, 2015

Stratification of surface waters during the last glacial millennial climatic events

M. Wary et al.